The Use of FDTD for the Analysis of Magnetoplasma Channel Waveguides

Rubem Gonçalves Farias and Attílio José Giarola, *Life Senior Member, IEEE*

***Abstract*— The finite-difference time-domain (FDTD) method is used for the analysis of magnetoplasma rectangular channel waveguides. Single and parallel-coupled waveguides are considered. The effect of varying the amplitude and the orientation of the bias magnetic field B_0 on the dispersion characteristics of the first modes is examined. However, the FDTD formulation, does not excite evanescent modes for a sufficiently long time interval, particularly when in the presence of the propagating or dynamic modes. As a result, the nonreciprocal properties of these structures, primarily associated with the evanescent modes, could not be investigated.**

***Index Terms*—Dispersion characteristics, FDTD method, magnetoplasma channel waveguides.**

I. Introduction

THE GROWING demand for signal processing at very high rates has enhanced the interest in the millimeter-wave band technology. Dielectric waveguides are particularly attractive for use in this frequency band because of their better performance than other waveguides, including those containing metallic elements, such as microstrip lines and finlines. The possibility of controlling the propagation characteristics of these waveguides has suggested the use of a plasma-induced semiconductor, controlled by a magnetic field [1], [2]. Single and parallel-coupled rectangular channel waveguides, as shown in Figs. 1 and 2, respectively, were, therefore, considered with the dielectric replaced by a semiconductor. To keep the losses low, a lightly doped semiconductor was chosen.

The magnetoplasma was induced by means of a magnetic field B_0 applied along a general orientation. To study the effect of the amplitude and orientation of B_0 on the propagation characteristics along the magnetoplasma rectangular channel waveguide, a finite-difference time-domain (FDTD) formulation was developed. This formulation is highly complex, primarily due to the discretized version of the convolution between the electric susceptibility in the time domain $\chi(t)$ and the electric field. This convolution is done by iteration, similar to the procedure followed by Luebbers *et al.* [3]. With the general orientation of B_0, the electric susceptibility is a tensor that may have all nine elements different from zero. In addition, each tensor element may simultaneously have

Manuscript received April 8, 1996; revised September 1, 1997. This work was supported by CNPq, FAPESP, TELEBRÁS, and FINEP.

R. G. Farias is with the Electrical Engineering Department, Federal University of Pará (UFPa), Belém, PA, Brazil CEDEX 66075-900.

A. J. Giarola is with the School of Electrical Engineering, State University of Campinas (UNICAMP), Campinas, SP, Brazil CEDEX 13083-970.

Publisher Item Identifier S 0018-9480(98)02754-9.

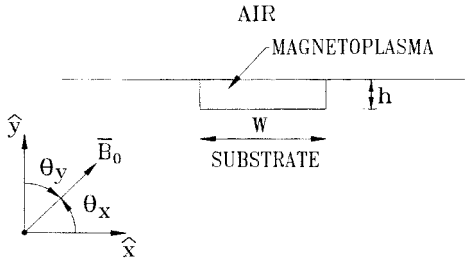

Fig. 1. Single rectangular channel waveguide.

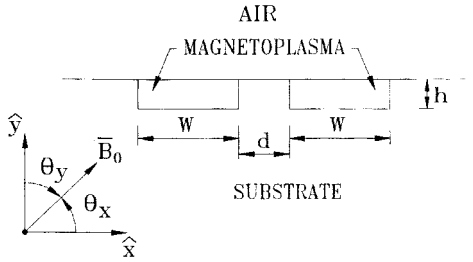

Fig. 2. Parallel-coupled rectangular channel waveguide.

Debye and Lorentz poles. The complexity of the formulation could be even higher if more than one type of carrier were considered in the semiconductor. The examples shown here consider only the case of a lightly doped N-type GaAs semiconductor. Therefore, only one type of carrier is sufficient for this analysis.

II. The Time Discretization of Maxwell's Equations

For normalized electromagnetic fields with the free-space intrinsic impedance equal to unity, the curl Maxwell's equations for a medium with a relative permeability $\mu_r = 1$ are written as

$$\frac{\partial \mathbf{C}}{\partial t} + \varepsilon_s \frac{\partial \mathbf{E}}{\partial t} = c\nabla \times \mathbf{H} \tag{1}$$

$$\frac{\partial \mathbf{H}}{\partial t} = -c\nabla \times \mathbf{E} \tag{2}$$

where $\mathbf{C}$ is the convolution vector

$$\mathbf{C} = \overline{\overline{\chi}}(t) \otimes \overline{E} \tag{3}$$

ε_s is the static dielectric constant, c is the velocity of light in free space, and $\overline{\overline{\chi}}(t)$ is the time-dependent electric-susceptibility tensor. $\mathbf{E}$ and $\mathbf{H}$ are the electric- and magnetic-field vectors, respectively.

The notation introduced by Yee [5] is also used here such that a field vector $\mathbf{W}(t)$ in an instant $t = n\delta t$ is abbreviated by $\mathbf{W}^n$ where δt is the time increment between two consecutive $\mathbf{E}$ field samples. The time interval between consecutive samples of $\mathbf{E}$ and $\mathbf{H}$ fields is equal to $\frac{1}{2}\delta t$.

After time discretization, the following system of equations is obtained from Maxwell's equations (1) and (2):

$$\mathbf{H}^{n+1/2} = \mathbf{H}^{n-1/2} - \mathbf{R}_e^n \tag{4}$$

$$\mathbf{C}^{n+1} + \varepsilon_s \mathbf{E}^{n+1} = \mathbf{C}^n + \varepsilon_s \mathbf{E}^n + \mathbf{R}_h^{n+1/2} \tag{5}$$

where $\mathbf{R}_e$ and $\mathbf{R}_h$ are the auxiliary curl fields, defined by

$$\mathbf{R}_e = \mathrm{c}\delta\mathrm{t} \nabla \times \mathbf{E} \tag{6}$$

$$\mathbf{R}_h = \mathrm{c}\delta\mathrm{t} \nabla \times \mathbf{H}. \tag{7}$$

Note that $\mathbf{H}^{n+1/2}$ is explicitly obtained from (4). Because $\mathbf{C}^{n+1}$ contains terms in $\mathbf{E}^{n+1}$, $\mathbf{E}^n$, $\mathbf{E}^{n-1}, \cdots, \mathbf{E}^1$ then $\mathbf{E}^{n+1}$ cannot be explicitly obtained from (5). It is necessary, therefore, to obtain a relation between $\mathbf{C}^{n+1}$ and $\mathbf{E}^{n+1}$.

Following Luebbers *et al.* [3], and because the variation of $\mathbf{E}(t)$ in comparison with $\overline{\overline{\chi}}(t)$ in a time interval δt is small, then

$$\begin{aligned}\mathbf{C}^n &= \int_0^t \overline{\overline{\chi}}(t-\tau)\mathbf{E}(\tau)d\tau\Big|_{t=n\delta t} \\ &\cong \sum_{m=0}^{n-1}\left\{\left[\int_{m\delta t}^{(m+1)\delta t} \overline{\overline{\chi}}\tau)d\tau\right]E^{n-m}\right\}.\end{aligned} \tag{8}$$

The following definitions are made:

$$\overline{\overline{\chi}}^0 = \int_0^{\delta_t} \overline{\overline{\chi}}(\tau)\, d\tau \tag{9}$$

$$\overline{\overline{\chi}}^m = \int_{m\delta t}^{(m+1)\delta_t} \overline{\overline{\chi}}(\tau)\, d\tau \tag{10}$$

$$\Delta\overline{\overline{\chi}}^m = \overline{\overline{\chi}}^m - \overline{\overline{\chi}}^{m+1} \tag{11}$$

$$\overline{\Psi}^n = \sum_{m=0}^{n-1} \Delta\overline{\overline{\chi}}^m \mathbf{E}^{n-m}. \tag{12}$$

The convolution vector $\mathbf{C}^{n+1}$ may, therefore, be written as

$$\mathbf{C}^{n+1} = \overline{\overline{\chi}}^0 \mathbf{E}^{n+1} + \mathbf{C}^n + \boldsymbol{\Psi}^n. \tag{13}$$

From (5) and (13), $\mathbf{E}^{n+1}$ is explicitly obtained from

$$\mathbf{E}^{n+1} = (\varepsilon_s \overline{\overline{I}} + \overline{\overline{\chi}}^0)^{-1}(\varepsilon_s \mathbf{E}^n + \boldsymbol{\Psi}^n + \mathbf{R}_h^{n+1/2}) \tag{14}$$

where $\overline{\overline{I}}$ is the idem factor and $(\cdot)^{-1}$ is the inverse matrix of $(\cdot)$.

The convolution difference vector $\overline{\Psi}^n$ may be expressed in terms of its basic components as

$$\overline{\Psi}^n = \begin{pmatrix}\Psi_x^n \\ \Psi_y^n \\ \Psi_z^n\end{pmatrix} = \begin{pmatrix}\Psi_{xx}^n + \Psi_{xy}^n + \Psi_{xz}^n \\ \Psi_{yx}^n + \Psi_{yy}^n + \Psi_{yz}^n \\ \Psi_{zx}^n + \Psi_{zy}^n + \Psi_{zz}^n\end{pmatrix} \tag{15}$$

where

$$\Psi_{uv}^n = \sum_{m=0}^{n-1} \Delta\chi_{uv}^m E_u^{n-m}, \qquad u, v = x, y, z. \tag{16}$$

For magnetization along an arbitrary direction, the susceptibility tensor elements for a given carrier k are given by

$$\begin{aligned}\chi_{k_{uv}}(t) = \chi_{s_{k_{uv}}}\{1 + K_{1_{k_{uv}}} e^{-\nu_k t} + [K_{2_{k_{uv}}} \cos(\omega_{c_k} t) \\ + K_{3_{k_{uv}}} \sin(\omega_{c_k} t)]e^{-\nu_k t}\}U(t), \\ u, v = x, yz\end{aligned} \tag{17}$$

where $U(t)$ is the unit step function and

$$\begin{aligned}\chi_{s_{k_{uu}}} &= (\varepsilon_s \omega_{pk}^2)\frac{\nu_k^2 + \omega_{c_{k_u}}^2}{\nu_k(\nu_k^2 + \omega_{c_k}^2)} \\ K_{1_{k_{uu}}} &= -\left(\frac{\omega_{c_{k_u}}^2}{\omega_{c_k}^2}\right)\frac{\nu_k^2 + \omega_{c_k}^2}{\nu_k^2 + \omega_{c_{k_u}}^2} \\ K_{2_{k_{uu}}} &= -\left(\frac{\nu_k^2}{\omega_{c_k}^2}\right)\frac{\omega_{c_k}^2 - \omega_{c_{k_u}}^2}{\nu_k^2 + \omega_{c_{k_u}}^2} \\ K_{3_{k_{uu}}} &= \left(\frac{\nu_k}{\omega_{c_k}}\right)\frac{\omega_{c_k}^2 - \omega_{c_{k_u}}^2}{\nu_k^2 + \omega_{c_{k_u}}^2} \\ \chi_{s_{k_{uv}}} &= (\varepsilon_s \omega_{pk}^2)\frac{b_{k_{uv}}}{\nu_k(\nu_k^2 + \omega_{c_k}^2)} \\ K_{1_{k_{uv}}} &= \left(\frac{\nu_k^2 + \omega_{c_k}^2}{\omega_{c_k}^2}\right)\left(\nu_k \frac{a_{k_{uv}}}{b_{k_{uv}}} - 1\right) \\ K_{2_{k_{uv}}} &= \frac{\nu_k^2}{\omega_{c_k}^2}\left[1 - \frac{\nu_k^2 + \omega_{c_k}^2}{\nu_k}\left(\frac{a_{k_{uv}}}{b_{k_{uv}}}\right)\right] \\ K_{3_{k_{uv}}} &= -\frac{\nu_k}{\omega_{ck}}, \qquad \text{for } u \neq v\end{aligned} \tag{18}$$

with the parameters $a_{k_{uv}}$ and $b_{k_{uv}}$ given by

$$\begin{aligned}&a_{k_{xy}} = -\omega_{c_{k_z}} \quad a_{k_{yz}} = -\omega_{c_{k_x}} \quad a_{k_{zx}} = -\omega_{c_{k_y}} \\ &a_{k_{yx}} = \omega_{c_{k_z}} \quad a_{k_{zy}} = \omega_{c_{k_x}} \quad a_{k_{xz}} = \omega_{c_{k_y}} \\ &b_{k_{xy}} = \omega_{c_{k_x}}\omega_{c_{k_y}} - \nu_k\omega_{c_{k_z}} \quad b_{k_{yz}} = \omega_{c_{k_y}}\omega_{c_{k_z}} - \nu_k\omega_{c_{k_x}} \\ &b_{k_{zx}} = \omega_{c_{k_z}}\omega_{c_{k_x}} - \nu_k\omega_{c_{k_y}} \quad b_{k_{yx}} = \omega_{c_{k_y}}\omega_{c_{k_x}} + \nu_k\omega_{c_{k_z}} \\ &b_{k_{zy}} = \omega_{c_{k_z}}\omega_{c_{k_y}} + \nu_k\omega_{c_{k_x}} \quad b_{k_{xz}} = \omega_{c_{k_x}}\omega_{c_{k_z}} + \nu_k\omega_{c_{k_y}}\end{aligned} \tag{19}$$

and with the cyclotron frequency ω_{c_k} and plasma frequency ω_{p_k} of the carrier k given by

$$\omega_{c_k} = \frac{q_k B_0}{m_k^*} \quad \omega_{p_k} = \left(\frac{q_k^2 N_k}{\varepsilon_0 \varepsilon_s m_k^*}\right)^{1/2} \tag{20}$$

where q_k is the charge, m_k^* is the effective mass, N_k is the carrier concentration, and ν_k is the collision rate of carrier k.

The susceptibility tensor $\overline{\overline{\chi}}(t)$ of the semiconductor with K_c type of carriers (electrons and holes from doping, photoinduced electrons and holes, etc.) is given by

$$\overline{\overline{\chi}}(t) = \sum_{k=1}^{K_c} \overline{\overline{\chi}}_k(t). \tag{21}$$

In order to obtain the iterative calculation of the convolution difference, $\chi_{k_{uv}}(t)$ should be an exponential function [3]. This is accomplished by defining a complex version of (17) as follows:

$$\hat{\chi}_{k_{uv}}(t) = [1 + K_{1_{k_{uv}}} e^{-\nu_k t} + (K_{2_{k_{uv}}} + jK_{3_{k_{uv}}})e^{-\hat{\gamma}_k t}]U(t) \tag{22}$$

where $\hat{\gamma}_k = \nu_k + j\omega_{c_k}$ with $j = \sqrt{-1}$, such that

$$\chi_{k_{uv}}(t) = R\{\hat{\chi}_{k_{uv}}(t)\} \tag{23}$$

$R\{\hat{\chi}\}$ representing the real part of $\hat{\chi}$.

The discretized version of the convolution difference is, therefore, obtained from

$$\boldsymbol{\Psi}_k^n = R\{\overline{\hat{\Psi}}_k^n\} = \boldsymbol{\Psi}_{R_k}^n + R\{\overline{\hat{\Psi}}_{C_k}^n\} \tag{24}$$

where

$$\boldsymbol{\Psi}_{R_k}^n = \left[\frac{(\overline{\overline{\chi_{s_k} K_{1_k}}})}{\gamma_k}(1 - e^{-\gamma_k \delta t})^2\right]\mathbf{E}^n + e^{-\nu_k \delta t}\boldsymbol{\Psi}_{R_k}^{n-1} \tag{25}$$

$$\overline{\hat{\Psi}}_{C_k}^n = \left[\frac{(\overline{\overline{\chi_{s_k} K_{2_k}}}) + j(\overline{\overline{\chi_{s_k} K_{3_k}}})}{\hat{\gamma}}(1 - e^{-\hat{\gamma}_k \delta t})^2\right]\mathbf{E}^n + e^{-\hat{\gamma}_k \delta t}\overline{\hat{\Psi}}_{C_k}^{n-1} \tag{26}$$

with

$$\boldsymbol{\Psi}_{R_k}^n = \sum_{m=0}^{n-1}\left[\frac{(\overline{\overline{\chi_{s_k} K_{1_k}}})}{\gamma_k}(1 - e^{-\nu_k \delta t})^2 e^{-m\nu_k \delta t}\right]\mathbf{E}^{n-m} \tag{27}$$

$$\overline{\hat{\Psi}}_{C_k}^n = \sum_{m=0}^{n-1}\left[\frac{(\overline{\overline{\chi_{s_k} K_{2_k}}}) + j(\overline{\overline{\chi_{s_k} K_{3_k}}})}{\hat{\gamma}_k} \cdot (1 - e^{-\overline{\gamma}_k \delta t})^2 e^{-m\nu_k \delta t}\right]\mathbf{E}^{n-m}. \tag{28}$$

III. 3-D Space Discretization

Yee's cell [5] will be used for the three-dimensional space discretization (3D-FDTD). The general location of each cell in a Cartesian coordinate system is represented by $(I, J, K) \rightarrow (I\delta x, J\delta y, K\delta z)$, where I, J, and K are integer numbers and δx, δy, and δz are the cell dimensions along $\hat{x}$, $\hat{y}$, and $\hat{z}$, respectively. The notation for any field component $W(x, y, z, t)$ after time and space discretization is, therefore,

$$W(x, y, z, t) \cong W(I\delta x, J\delta y, K\delta z, n\delta t) \rightarrow W^n(I, J, K).$$

For each spatial cell, there are six field components. For example, for a cell with a location (I, J, K) these components are

$$E_x^n\left(I + \frac{1}{2}, J, K\right)$$
$$E_y^n\left(I, J + \frac{1}{2}, K\right)$$
$$E_z^n\left(I, J, K + \frac{1}{2}\right)$$
$$H_x^{n+1/2}\left(I, J + \frac{1}{2}, K + \frac{1}{2}\right)$$
$$H_y^{n+1/2}\left(I + \frac{1}{2}, J, K + \frac{1}{2}\right)$$
$$H_z^{n+1/2}\left(I + \frac{1}{2}, J + \frac{1}{2}, K\right).$$

The six auxiliary curl field components are (29)–(34), shown at the bottom of the page, where the parameters S_x,

$$R_{ex}^n(I, J, K) = S_y\left[E_z^n\left(I, J+1, K+\frac{1}{2}\right) - E_z^n\left(I, J, K+\frac{1}{2}\right)\right] - S_z\left[E_y^n\left(I, J+\frac{1}{2}, K+1\right) - E_y^n\left(I, J+\frac{1}{2}, K\right)\right] \tag{29}$$

$$R_{ey}^n(I, J, K) = S_z\left[E_x^n\left(I+\frac{1}{2}, J, K+1\right) - E_x^n\left(I+\frac{1}{2}, J, K\right)\right] - S_x\left[E_z^n\left(I+1, J, K+\frac{1}{2}\right) - E_z^n\left(I, J, K+\frac{1}{2}\right)\right] \tag{30}$$

$$R_{ez}^n(I, J, K) = S_x\left[E_y^n\left(I+1, J+\frac{1}{2}, K\right) - E_y^n\left(I, J+\frac{1}{2}, K\right)\right] - S_y\left[E_x^n\left(I+\frac{1}{2}, J+1, K\right) - E_x^n\left(I+\frac{1}{2}, J, K\right)\right] \tag{31}$$

$$R_{hx}^{n+1/2}(I, J, K) = S_y\left[H_z^{n+1/2}\left(I+\frac{1}{2}, J+\frac{1}{2}, K\right) - H_z^{n+1/2}\left(I+\frac{1}{2}, J-\frac{1}{2}, K\right)\right] - S_z\left[H_y^{n+1/2}\left(I+\frac{1}{2}, J, K+\frac{1}{2}\right) - H_y^{n+1/2}\left(I+\frac{1}{2}, J, K-\frac{1}{2}\right)\right] \tag{32}$$

$$R_{hy}^{n+1/2}(I, J, K) = S_z\left[H_x^{n+1/2}\left(I, J+\frac{1}{2}, K+\frac{1}{2}\right) - H_x^{n+1/2}\left(I, J+\frac{1}{2}, K-\frac{1}{2}\right)\right] - S_x\left[H_z^{n+1/2}\left(I+\frac{1}{2}, J+\frac{1}{2}, K\right) - H_z^{n+1/2}\left(I-\frac{1}{2}, J+\frac{1}{2}, K\right)\right] \tag{33}$$

$$R_{hz}^{n+1/2}(I, J, K) = S_x\left[H_y^{n+1/2}\left(I+\frac{1}{2}, J, K+\frac{1}{2}\right) - H_y^{n+1/2}\left(I-\frac{1}{2}, J, K+\frac{1}{2}\right)\right] - S_y\left[H_x^{n+1/2}\left(I, J+\frac{1}{2}, K+\frac{1}{2}\right) - H_x^{n+1/2}\left(I, J-\frac{1}{2}, K+\frac{1}{2}\right)\right] \tag{34}$$

S_y, and S_z are defined by

$$S_x = S_x(I, J, K) = \frac{c\delta t}{\delta_x(I, J, K)} \tag{35}$$

$$S_y = S_y(I, J, K) = \frac{c\delta t}{\delta_y(I, J, K)} \tag{36}$$

$$S_z = S_z(I, J, K) = \frac{c\delta t}{\delta_z(I, J, K)} \tag{37}$$

IV. 2-D Space Discretization

For a uniform waveguide along the z-direction, the fields propagate with an amplitude proportional to $\exp(-j\beta z)$, where β is the phase constant of the propagating mode. Due to this exponential dependence on z, the derivative of any field component with respect to z may be replaced by $-j\beta$. The problem may, therefore, be treated as a two-dimensional space discretization (2-D FDTD).

The expressions for $\mathbf{R}_e^n(I, J)$ and $\mathbf{R}_h^{n+1/2}(I, J)$ are then reduced to (38)-(43), shown at the bottom of the page, where

$$S_x = \frac{c\delta t}{\delta_x(I, J)} \quad S_y = \frac{c\delta t}{\delta_y(I, J)} \quad S_z = jc\delta t\beta. \tag{44}$$

Note that S_z is a parameter that depends directly of the phase constant β, which is treated as an input parameter for the 2-D FDTD.

Only Gaussian excitations in time and space are considered here, and are expressed by

$$W_s(x, y, t) + \Phi(x, y)[e^{-(t-t_1)^2/2\sigma_t^2} - e^{-(t-t_2)^2/2\sigma_t^2}] \tag{45}$$

with

$$\Phi(x, y) = W_0 e^{-(x-x_0)^2/2\sigma_x^2} - e^{-(y-y_0)^2/2\sigma_y^2}. \tag{46}$$

The excitation pulse W_s is truncated at a time $t = t_s$, sufficiently large in order to avoid an abrupt variation in the excitation pulse. The values used in most of the simulations were $t_1 = 3.7\sigma_t$, $t_2 = 2t_1$, and $t_s = 3t_1$. The space distribution of $W_s(x, y, t)$ is applied to the center of the waveguide core, with polarization along $\hat{x}$ for the E_{11}^x mode, and along $\hat{y}$ for the E_{11}^y mode.

The maximum time increment $\delta t_{\max}$ based on the Courant condition for the 2-D FDTD is

$$\delta t_{\max} = \frac{n_{\min}}{c\sqrt{2(1/\delta_{\min})^2 + (\beta/2)^2}} \tag{47}$$

where $n_{\min}$ is the smallest value of refraction index of the materials in the waveguide and $\delta_{\min}$ is the smallest space increment used.

An adequate choice of time increment is $\delta t = c_t \delta t_{\max}$, with $c_t \leq 1$. For $c_t > 1$, instabilities are usually observed. A convenient choice is $c_t = 1$ because higher dispersion errors are observed with lower values of c_t [7].

To limit the computational domain, three types of walls are considered: electric, magnetic, and absorbing. In the electric wall, the tangential component of the electric field is set equal to zero, while in the magnetic wall the tangential component of the magnetic field is set equal to zero. In the absorbing wall, the first-order Mur's approximation [8] is used. This approximation is sufficient for the examples considered here.

V. Numerical Results

Single and parallel-coupled rectangular channel waveguides (as shown in Figs. 1 and 2, respectively), are considered here. The core consists of a lightly doped n-type GaAs semiconductor biased by means of a static magnetic field B_0 along an arbitrary $\hat{u}$-direction. A magnetoplasma is thus induced in the core.

The numerical results shown here were calculated with the following material and geometrical parameters:

1) cyclotron frequency: $f_c = 10$, 30, 60, 90, or 120 GHz ($B_0 \cong 235$, 705, 1411, 2116, or 2822 G);
2) plasma frequency: $f_p = 30$ GHz ($N \cong 9.4 \times 10^{12}$ cm^{-3});
3) collision rate: $\nu = 125.7 \times 10^9$ collisions/s ($\tau = 7.96$ ps);
4) dielectric constant of the plasma host (GaAs): $\varepsilon_s = 12.0$;
5) dielectric constant of the substrate: $\varepsilon_{\text{sub}} = 2.25$;
6) effective mass of the carrier: $m^* = 0.07$ m$_0$;
7) channel height: $h = 1.0$ mm;
8) channel width: $w = 2.0$ mm;

$$R_{ex}^n(I, J) = S_y[E_z^n(I, J+1) - E_z^n(I, J)] + S_z E_y^n\left(I, J+\frac{1}{2}\right) \tag{38}$$

$$R_{ey}^n(I, J) = -S_z E_x^n\left(I+\frac{1}{2}, J\right) - S_x[E_z^n(I+1, J) - E_z^n(I, J)] \tag{39}$$

$$R_{ez}^n(I, J) = S_x\left[E_y^n\left(I+1, J+\frac{1}{2}\right) - E_y^n\left(I, J+\frac{1}{2}\right)\right] - S_y\left[E_x^n\left(I+\frac{1}{2}, J+1\right) - E_x^n\left(I+\frac{1}{2}, J\right)\right] \tag{40}$$

$$R_{hx}^{n+1/2}(I, J) = S_y\left[H_z^{n+1/2}\left(I+\frac{1}{2}, J+\frac{1}{2}\right) - H_z^{n+1/2}\left(I+\frac{1}{2}, J-\frac{1}{2}\right)\right] + S_z H_y^{n+1/2}\left(I+\frac{1}{2}, J\right) \tag{41}$$

$$R_{hy}^{n+1/2}(I, J) = -S_z H_x^{n+1/2}\left(I, J+\frac{1}{2}\right) - S_x\left[H_z^{n+1/2}\left(I+\frac{1}{2}, J+\frac{1}{2}\right) - H_z^{n+1/2}\left(I-\frac{1}{2}, J+\frac{1}{2}\right)\right] \tag{42}$$

$$R_{hz}^{n+1/2}(I, J) = S_x\left[H_y^{n+1/2}\left(I+\frac{1}{2}, J\right) - H_y^{n+1/2}\left(I-\frac{1}{2}, J\right)\right] - S_y\left[H_x^{n+1/2}\left(I, J+\frac{1}{2}\right) - H_x^{n+12}\left(I, J-\frac{1}{2}\right)\right] \tag{43}$$

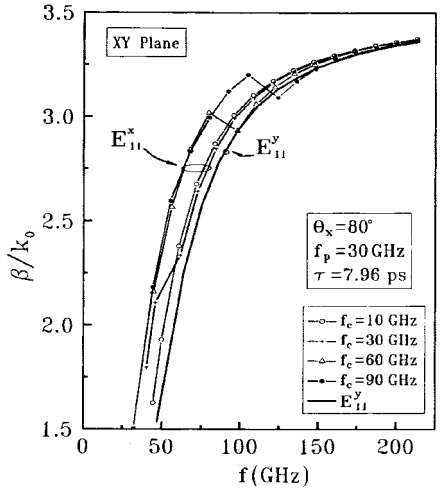

Fig. 3. Effect of f_c on the dispersion characteristics of the E^x_{11} and E^y_{11} modes.

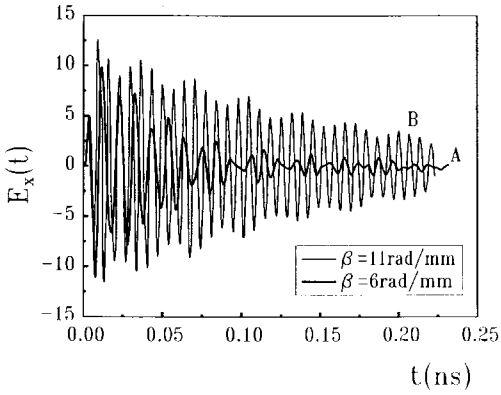

Fig. 4. Time response of $E_x(t)$, for $\beta = 6$ and 11 rd/mm, showing the strong effect of the gyroresonance on the attenuation of the dominant E^x_{11} mode.

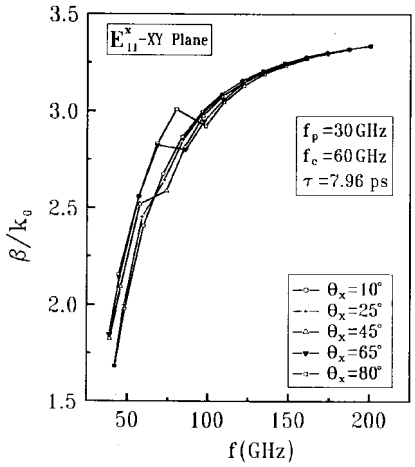

Fig. 5. Effect of θ_x on the dispersion characteristics of the E^x_{11} mode.

9) minimum dimension of space discretization $\delta_{\min} = 0.1$ mm;
10) spatial width in rms of the excitation pulse: $\sigma_x = 0.56$ mm;
11) spatial height in rms of the excitation pulse: $\sigma_y = 0.28$ mm;
12) spectral bandwidth of the excitation pulse: $B_f = 220$ GHz;
13) number of time iterations for each modal point (β, ω): $n_T = 1001$;
14) phase constants at which the modal points (β, ω) were calculated: $\beta = 1.5, 2, 3, \cdots, 14$ rad/mm.

A. Single Rectangular Channel Waveguide

Besides the previously mentioned parameters, the following were additionally chosen for the single rectangular channel waveguide of Fig. 1:

1) numerical domain width: $L_x = 6.0$ mm;
2) numerical domain height: $L_y = 5.0$ mm;
3) number of cells along the horizontal axis: $n_x = 44$;
4) number of cells along the vertical axis: $n_y = 34$.

The effect of f_c on the dispersive characteristics of E^x_{11} and E^y_{11} modes is shown in Fig. 3 for an angle between $B_0\hat{u}$ and $\hat{x}$, given by $\theta_x = 80°$. Since the E^y_{11} mode has the electric-field component nearly aligned with the static magnetic field B_0, the Lorentz force is very weak such that the dispersion curve is practically unaffected by f_c. However, for the E^x_{11} mode, not only is the electric field nearly perpendicular to the static magnetic field, but also both the electric and static magnetic fields are perpendicular to the direction of mode propagation. This situation is known as the Voight-type configuration [9]. Note that the effect of the static magnetic field is pronounced and causes gyroresonances, which are essentially dependent on f_c, f_p, and θ_x. These resonances are associated with the transitions observed in Fig. 3. The attenuation caused by the magnetic resonances is better observed in the time responses of the electric field shown in Fig. 4 for $f_c = 60$ GHz and for two values of $\beta = 6$ and 11 rd/mm. The high attenuation observed for $\beta = 6$ rad/mm is due to the resonance. For $\beta = 11$ rad/mm, the attenuation is not as high and it is due to the collision rate of the carriers in the plasma. The observed mode composition is due to the excitation of a higher order mode. Not only the transition caused by the plasma resonance, but also the excitation of higher order modes makes the calculation of the wave attenuation very difficult by the FDTD method.

The effect of the orientation of B_0 on the dispersion curves of the waveguide are shown in Figs. 5 and 6. As may be observed in Fig. 5, for $\theta_x = 10°$, the curve for the E^x_{11} mode is practically unaffected by the presence of B_0. The effect, however, becomes more pronounced when θ_x increases and it nearly saturates at $\theta_x = 65°$. Note also, that the transitions are more abrupt at the higher values of θ_x. Fig. 6 shows that the effect, not only on the E^x_{11} mode, but also on the E^y_{11} mode, is very small when θ_z is varied in the zx-plane. Similar results were also observed in the zy-plane.

For the Voight-type configuration, with crossed RF and B_0 fields, the propagation characteristics may become quite complex, particularly with strong B_0 fields, as shown in Fig. 7. This type of behavior is similar to that described by Bolle and Talisa [1]. The FDTD algorithm developed here, however, excites well only the propagating or dynamic modes. The evanescent modes are not excited for a sufficiently

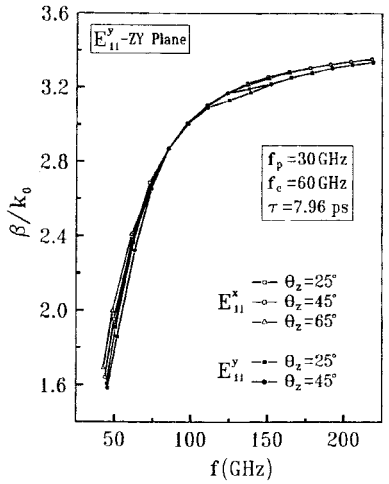

Fig. 6. Effect of θ_z on the dispersion characteristics of the E^x_{11} and E^y_{11} modes.

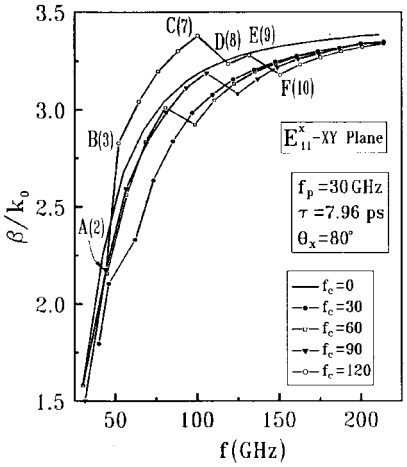

Fig. 7. Effect of the amplitude of B_0 on the dispersion characteristics of the E^x_{11} mode in a Voight-type configuration.

long period of time when they are in the presence of the dynamic modes. They cannot, therefore, be observed. As a result, the nonreciprocal effects in magnetoplasma rectangular waveguides primarily associated with the evanescent modes could not be observed using the FDTD formulation.

In order to obtain the results shown here, the numerical domain was segmented in various regions and the discretization was done with a concentration at the materials interfaces. The waveguide core was uniformly discretized while in other regions the discretization was gradually done, such that the increase in cells dimensions was done in a direction of decreasing effective values of the dominant component of the electric field. For each material interface side, the cells dimensions were made equal to a value of $\delta_{\min}$.

Fig. 8 shows the behavior of the cells width in millimeters along the horizontal axis that passes through the waveguide-core center of gravity. A similar procedure is followed for a direction along the vertical axis. In this figure, three refinement degrees are shown and are indicated by *c*, *d*, and *e*. The values of $\delta_{\min}$ are given by 100, 80, and 65 μm, respectively. The arrows indicate the materials interfaces.

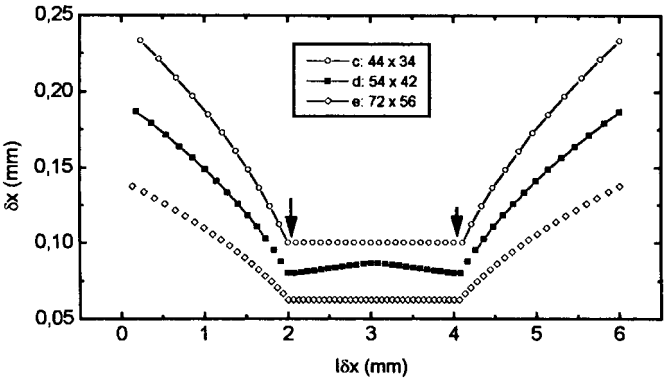

Fig. 8. Spatial configuration for three degrees of numerical domain refinements.

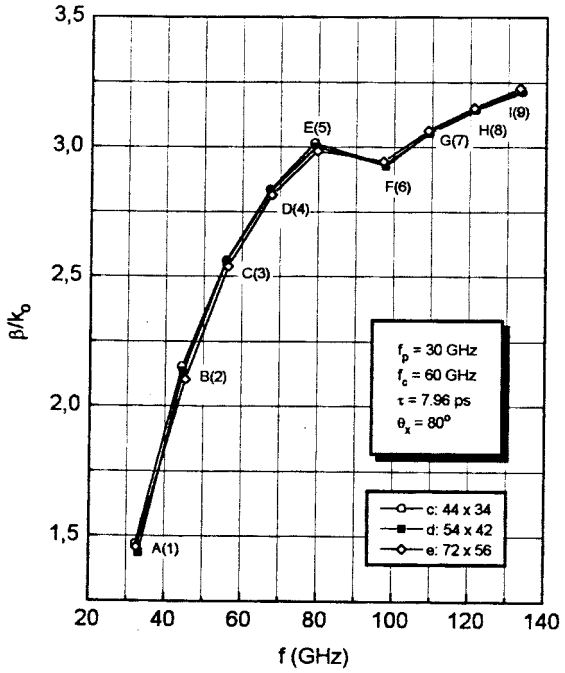

Fig. 9. Propagation characteristics with the three degrees of numerical domain refinements of Fig. 8.

Fig. 9 shows the dispersion characteristics with the three above-mentioned refinement degrees. Note that there is only a very small deviation between solutions. Option c: 44 × 34 was used for the results shown here, for which the numerical domain discretization consists of 44 cells along the horizontal axis x, and 34 cells along the vertical axis y.

In order to clarify the region of transition caused by the plasma resonance, consider the points $E(5)$ and $F(6)$ of Fig. 9. The numbers 5 and 6 (between parenthesis) are used to indicate the value of β, expressed in rd/mm. The electric-field spectra for these values of β are shown in Fig. 10. Also shown in this figure (in a heavy solid trace) is the spectrum for an intermediate value $\beta = 5.5$ rd/mm. In this case, the presence of both modes is well characterized by the two peaks indicated by the arrows. In some cases, even three modes may be observed simultaneously, as is the case of $\beta = 5.0$ rd/mm, shown by the light solid trace of Fig. 10. This effect may be explained by making a correlation with the solutions obtained by Davies *et al.* [10], particularly with their results shown in Figs. 4 and 5.

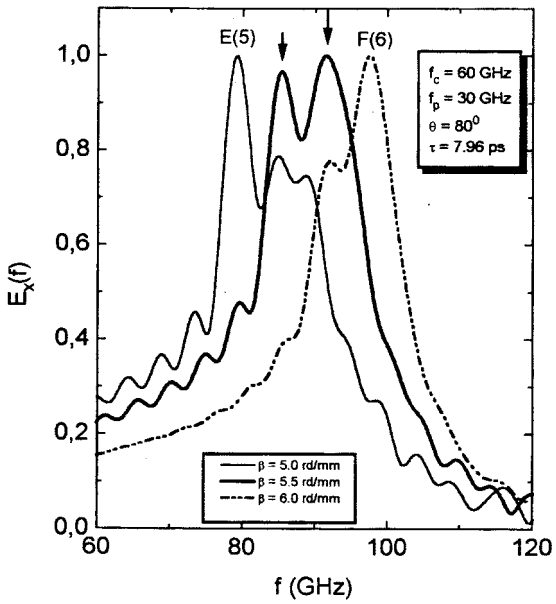

Fig. 10. Electric-field spectra for three values of β.

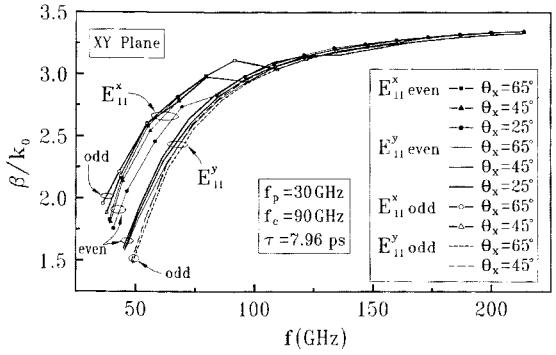

Fig. 11. Effect of θ_x on the dispersion characteristics of the even and odd E_{11}^x and E_{11}^y modes.

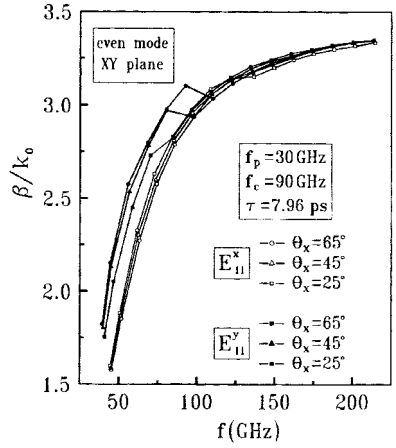

Fig. 12. Effect of θ_x on the dispersion characteristics of the even E_{11}^x and E_{11}^y modes.

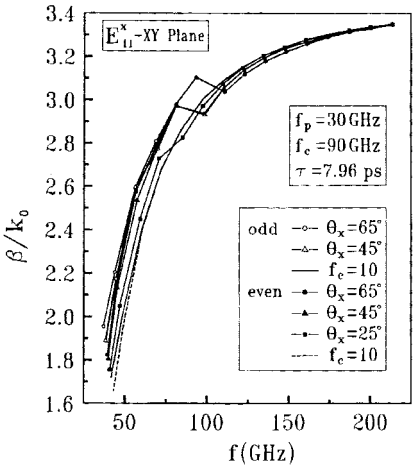

Fig. 13. Effect of θ_x on the dispersion characteristics of the even and odd E_{11}^x modes for $f_c = 90$ GHz ($B_0 \cong 2116$ G). Also shown are curves for $f_c = 10$ GHz ($B_0 \cong 235$ G).

In order to test the validity for using the FDTD method to a magnetoplasma, results were obtained to compare with those shown by Harrington [11] using the moment method for the analysis of a metal cavity containing a magnetized plasma. A good agreement between the results from both methods was demonstrated [12]. In addition, convergence tests were done using various refinement degrees of discretization. The dispersion curves and field spectra were compared among themselves in order to arrive to the most satisfactory parameters for the discretization of the numeric domain.

B. Parallel-Coupled Rectangular Channel Waveguide

In addition to the geometrical and material parameters chosen in the beginning of this section, the following parameters were also used in the analysis of the parallel-coupled rectangular channel waveguide:

1) distance between channels: $d = 0.4$ mm;
2) numerical domain width: $L_x = 4.2$ mm;
3) numerical domain height: $L_y = 5.0$ mm;
4) number of cells along the horizontal axis: $n_x = 34$;
5) number of cells along the vertical axis: $n_y = 34$.

The effect of the orientation of B_0 on the dispersion curves of the even and odd E_{11}^x and E_{11}^y modes is shown in Figs. 11 and 12. As expected, most of the magnetization impact is verified in the even and odd E_{11}^x modes. The effect of θ_x on the dispersion characteristics of the even and odd E_{11}^y modes is small. In general, the magnetization causes a difference between the E_{11}^x and E_{11}^y modes that increases as θ_x is increased. In other words, the Lorentz force increases for the E_{11}^x mode and decreases for the E_{11}^y mode. This behavior is better observed in the curves for the even E_{11}^x and E_{11}^y modes, shown in Fig. 12. Note that the difference between propagation characteristics of even E_{11}^x and E_{11}^y modes is smaller for $\theta_x = 25°$. For $\theta_x = 65°$, the phase difference between even E_{11}^x and E_{11}^y modes is larger. In Fig. 13, the effect of orientation of the static magnetic field on the propagation characteristics of even and odd E_{11}^x modes is shown for $f_c = 90$ GHz ($B_0 \cong 2116$ G). Also shown are the curves for even and odd E_{11}^x modes with a residual magnetic field of approximately 235 G ($f_c = 10$ GHz). This static magnetic-field level is sufficiently low, such that its effect on the dispersion curves is negligible. Note that the effect of the static magnetic-field orientation on the phase

difference between these two modes is very small. This is because the phases of both modes change about the same amount when θ_x is varied. Consequently, only a small control of the coupling between waveguides is achieved by varying the orientation of the static magnetic field.

VI. Conclusions

An extended version of the FDTD method for the analysis of waveguides containing magnetoplasma was presented here. The derivative operator, not only in time, but also in space, was approximated by finite differences and applied directly to Maxwell's equations [5]. The formulation was extended by including the calculation of the convolution between the electric-field intensity and the electric-susceptibility tensor using a procedure similar to that described by Luebbers *et al.* [3]. This formulation is, therefore, applicable to waveguides containing magnetoplasma with a general orientation of the static magnetic field.

Numerical results for single and parallel-coupled magnetoplasma rectangular channel waveguides were presented. The effect of the amplitude and orientation of the static magnetic field on the dispersion characteristics of these waveguides was carefully examined. The nonreciprocal characteristics, however, could not be investigated because the FDTD formulation did not excite (for a sufficiently long time) the evanescent modes—the ones that are primarily responsible for this behavior.

References

[1] D. M. Bolle and S. H. Talisa, "Fundamental consideration in millimeter and nonmillimeter component design employing magnetoplasmons," *IEEE Trans. Microwave Theory Tech.*, vol. MTT-29, pp. 916–923, Sept. 1981.

[2] S. H. Talisa and D. M. Bolle, "Performance predictions for isolators and differential phase shifters for the near-millimeter wave range," *IEEE Trans. Microwave Theory Tech.*, vol. MTT-29, pp. 1338–1343, Dec. 1981.

[3] R. J. Luebbers, F. Hunsberger, and K. Kunz, "A frequency-dependent finite-difference time-domain formulation for transient propagation in plasma," *IEEE Trans. Antennas Propagat.*, vol. 39, pp. 29–34, Jan. 1991.

[4] F. Hunsberger, R. J. Luebbers, and K. Kunz, "Finite-difference time-domain analysis of gyrotropic media—I: Magnetized plasma," *IEEE Trans. Antennas Propagat.*, vol. 40, pp. 1489–1495, Dec. 1992.

[5] K. S. Yee, "Numerical solution of initial boundary value problems involving Maxwell's equations in isotropic media," *IEEE Trans. Antennas Propagat.*, vol. AP-14, pp. 302–307, May 1966.

[6] A. C. Cangellaris, "Numerical stability and numerical dispersion of a compact 2D-FDTD method used for the dispersion analysis of waveguides," *IEEE Microwave Guided Wave Lett.*, vol. 3, pp. 3–5, Jan. 1993.

[7] K. L. Shlager, J. G. Maloney, S. L. Ray, and A. F. Peterson, "Relative accuracy of several finite-difference time-domain methods in two and three dimensions," *IEEE Trans. Antennas Propagat.*, vol. 41, pp. 1732–1737, Dec. 1993.

[8] G. Mur, "Absorbing boundary conditions for the finite-difference approximation of the time-domain electromagnetic-field equations," *IEEE Trans. Electromag. Compat.*, vol. EMC-23, pp. 377–382, no. 1981.

[9] D. G. Swanson, *Plasma Waves.* New York: Academic, 1989.

[10] L. E. Davies, R. Sloan, and D. K. Paul, "T mom modes in transversely magnetized semiconductor-filled coaxial waveguide and parallel plates," *Proc. Inst. Elect. Eng.*, vol. 140, pt. H, no. 3, pp. 211–218, June 1993.

[11] R. F. Harrington, *Field Computation by Moments Methods.* Piscataway, NJ: IEEE Press, 1993, ch. 9.

[12] M. E. V. Segatto, R. G. Farias, and A. J. Giarola, "Electromagnetic wave propagation in waveguides with magnetized plasma," in *IEEE Antennas Propagat. Int. Symp. Dig.*, Newport Beach, CA, June 1995, pp. 652–655.

Rubem Gonçalves Farias was born in Afuá, PA, Brazil, in 1950. He received the B.S.E.E. degree from the Federal University of Parà (UFPA), Belém, Brazil, in 1974, the M.S. degree in electrical engineering from the Aeronautical Institute of Technology (ITA), São José dos Campos, São Paulo, Brazil, in 1983 and the Ph.D. degree from the State University of Campinas (UNICAMP), Campinas, São Paulo, Brazil, in 1996.

Since 1976, he has been a Professor in the Electrical Engineering Department, UFPA. His main interests are with microwave, millimeter-wave and optical-wave devices for communications. He is a member of the Microwave and Optoelectronics Brazilian Society (SBMO).

Dr. Farias received the Volkswagen/UFPA award in 1974 for his first-place graduation at the Technological Center, UFPA.

Attílio José Giarola (M'58–SM'76–LSM'95), was born in Brazil, in 1930. He received the B.S.E.E. degree from the University of São Paulo, Brazil, in 1954, and the M.S. and Ph.D. degrees from the University of Washington, Seattle, in 1959 and 1963, respectively.

He taught for several years at the Instituto Tecnológico de Aeronáutica (ITA), Brazil, Seattle University, and the University of Washington, prior to receiving the Ph.D. degree. In 1962, he joined the staff of the Boeing Company, Seattle, and was responsible for research on infrared detectors and microwave devices. He was an Associate Professor of electrical engineering at ITA and a Visiting Professor at the University of São Paulo, Brazil. During this time, he was the Program Chairman of the First National Electronics Conference in Brazil and conducted research in solid-state devices. From 1968 to 1974, he was an Associate Professor of electrical engineering at Texas A&M University, College Station, with responsibilities of teaching and conducting research on electromagnetics, particularly on electromagnetic susceptibility. In 1975, he joined the State University of Campinas (UNICAMP), Campinas, São Paulo, Brazil, where he was responsible for the implantation and development of a research program in antennas, microwave, and optical devices. From 1975 to 1987, he was the Dean of Graduate Studies, UNICAMP, and from 1980 to 1982, he was the Vice-President of Academic Affairs, UNICAMP. He is currently an Emeritus Professor at UNICAMP. He was the vice-president and president of the Brazilian Microwave and Optoelectronics Society (SBMO) and was chairman of the first SBMO International Symposium in 1985.

Dr. Giarola is a member of Eta Kappa Nu and Sigma Xi.